Study of particle dynamics and analysis using DDM microscopy

A Thesis

submitted to
Indian Institute of Science Education and Research Pune
in partial fulfillment of the requirements for the
BS-MS Dual Degree Programme

by

Surya Narayan Banerjee

Indian Institute of Science Education and Research Pune
Dr. Homi Bhabha Road,
Pashan, Pune 411008, INDIA.

April, 2021

Supervisor: Dr. G. V. Pavan Kumar, IISER Pune

Certificate

This is to certify that this dissertation entitled Study of particle dynamics and analysis using DDM microscopy towards the partial fulfilment of the BS-MS dual degree programme at the Indian Institute of Science Education and Research, Pune represents study/work carried out by Surya Narayan Banerjee at Indian Institute of Science Education and Research under the supervision of Dr. G. V. Pavan Kumar, IISER Pune, Associate Professor, Department of Physics , during the academic year 2020-2021.

Dr. G. V. Pavan Kumar, IISER Pune

Committee:

Dr. G. V. Pavan Kumar, IISER Pune

Dr. Vijayakumar Chikkadi, IISER Pune

This thesis is dedicated to my parents

Declaration

I hereby declare that the matter embodied in the report entitled Study of particle dynamics and analysis using DDM microscopy are the results of the work carried out by me at the Department of Physics, Indian Institute of Science Education and Research, Pune, under the supervision of Dr. G. V. Pavan Kumar, IISER Pune and the same has not been submitted elsewhere for any other degree.

Surya Narayan Banerjee

Acknowledgments

I would like to thank my guide and supervisor Prof.G.V. Pavan Kumar. He was the one who introduced me to this wonderful topic. He has been a constant source of learning and inspiration, in this lab. I would also like to thank my wonderful friend of 5 years and lab partner for the last year Utkarsh Khandelwal with whom i shared the initial journey of this thesis and he has been a constant help throughout this project. Without him, many of the experiments would not have been possible.I would also like to thank the other lab members name Shailendra Chaubey, Diptobroto Paul, Sunny Tiwary, Vandana Sharma and Chetna Taneja for their immensely valuable help and guidance, for taking time out of their busy schedules to help us learn any new experimental technique. Lab instrumentation calibrations would never have been posible for me without their thorough expertise. Finally I would like to thank my parents for giving me motivation to fight the odds and keep up to the challenges in life.There have been many others unnamed here but they all deserve my utmost respect as well, who have been involved with me both academically and on a friendly level.

Abstract

In plasmonics and nanophotonics, there are many techniques to study particle dynamics in a heterogeneous sample on a multi-length scale. In this thesis, we work towards making an optothermoelectric trap, and with self-preprepared plasmonic gold and silver nanoparticles and nanorods, attempt to study system dynamics using a revolutionary upcoming technique named Differential Dynamic Microscopy, which not only helps us to investigate the dynamics in spatial dimension but in time as well. We then study their related graphs and Fourier transform images and try to classify and quantify the various diffusive processes occurring in the system and get a picture of the dominating forces under various circumstances and their effects.

Contents

Abstract **xi**

1 Preliminaries **3**

1.1 Scattering 3

1.2 Trapping 8

1.3 Introduction to Differential Dynamic Microscopy 12

2 Preparation of Plasmonic Structures **17**

2.1 Preparation of Gold Nanoparticle 17

2.2 Preparation of Silver Nanoparticle 17

2.3 Preparation of Gold Nanoplate 18

3 Experiment And its Results **21**

3.1 Experimental setup 21

3.2 Experimental method 22

3.3 Observations and Results 25

4 Conclusion **43**

Introduction

Lasers have become an extremely important part of our scientific world in taking the technology ahead and the 2018 Nobel Prize in physics awarded to three pioneers of laser technology leaves no room for doubt about it. Among them, Arthur Ashkin received it for his revolutionary use in optical tweezers[1]. Since then, various types of tweezers be it optical, optothermal or optothermo-electric have been discovered, in order to trap, control and manipulate particles, of the order of microns down to nanoscale. These have huge applications in biological and physical sciences, e.g. studying biological activities down at the cellular level, drug delivery, nanotechnology and soft matter experiments and many more. Here we go on to recreate an advanced form of tweezer for soft matter in liquid phase, called otent traps, and then take the help of fourier imaging and a new technique called DDM to study our system of nanoparticles and their relative diffusion processes.

Chapter 1

Preliminaries

Here we take up some introductory topics and lay a theoretical basis fofr helping the readers to get a reference for the thesis, along with some essential phenomena and developments in photonics, leading to today's modern techniques.

1.1. Scattering

According to Britannica dictionary scattering is the change in direction of particle's movement caused due to obstruction from other particles, obstruction because there need not be a physical contact between the particles per se if there is enough dominant repulsive forces between them. In general, electromagnetic radiations also undergo the scattering phenomenon when interacting with both particles and surfaces, both of various kinds. The change in properties of the wave prior and after scattering depends on the medium and particles/surface. For eg. Light gets scattered on hitting various surfaces of physical objects all around us. With a charged particle though, it's different. The electromagnetic radiation puts a force on the charged particle. This force varies directly with the electric field. Thus the charged particle now starts moving according to the frequency of the radiation and in turn becomes source of secondary radiation. Now because energy is conserved, all the energy causing the particle's new motion is derived from the original radiation and this is called scattering. There are different types of scattering:

1.1.1 Rayleigh Scattering

This pertains to scattering of electromagnetic radiation from particles whose size is much smaller than the wavelength of the radiation. This type of scattering doesn't cause any gain in energy of the particle because there is no electronic excitation here, although there may be some Doppler shift, but that's it. In Raleigh scattering, the intensity of scattering is inversely proportional to the fourth power of wavelength. That is why Raleigh scattering[2] is so pronounced in shorter wavelengths. This strong wavelength dependence is what makes our day sky blue in colour, which is the lower end of the visible spectrum (lower in terms of wavelength). The smaller the wavelength, the more its scattering intensity, and hence bluer component is present in the sunlight which reaches the earth at a significant angle from the sun's direct rays. Raleigh scattering also happens due to the small dust particles inn air. Also, as priorly mentioned, Raleigh scattering is a form of elastic scattering i.e. the photon don't change energy before and after scattering off the small particles (small compared to the photon wavelength).

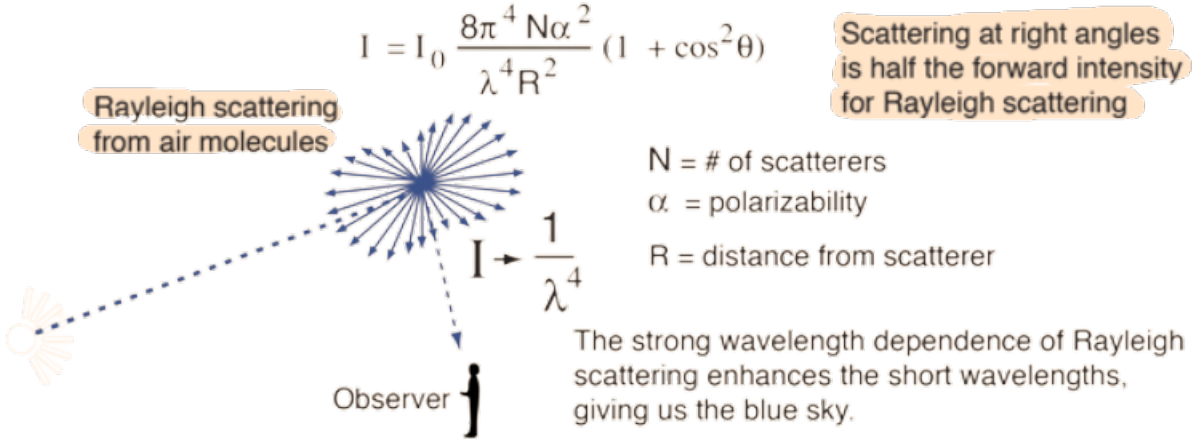

How Rayleigh scattering works [3]

We can also see that since the scattering intensity varies directly as $1 + \cos^2\theta$, the scattering in longitudinal direction (forward and backward scattering intensities) is much more than that in transverse direction, just like an induced dipole, which while oscillating in a direction perpendicular to its movement is unable to radiate along the direction of oscillation.[3]

1.1.2 Mie Scattering

: This type of scattering dominates when the particles are similar to or larger than the wavelength of the radiation[2]. Here there is a considerable change in optical phase over the course of scattering. As opposed to the Rayleigh scattering, here the scattering intensity doesn't depend strongly on the wavelength of radiation. This is what causes the white glare around the sun due to Mie scattering from the particulate matter present in the air, also the water droplets coalesced to form clouds are greyish white from this kind of scattering. Similarly, this scattering is also present in fat droplets and assigns milk its white colour. Mie scattering produces an antenna lobe-like pattern, with the forward scattering intensity being much more pronounced than the backward one because the relative phase difference of contributions from different scattering locations on the particles become smaller.[3]

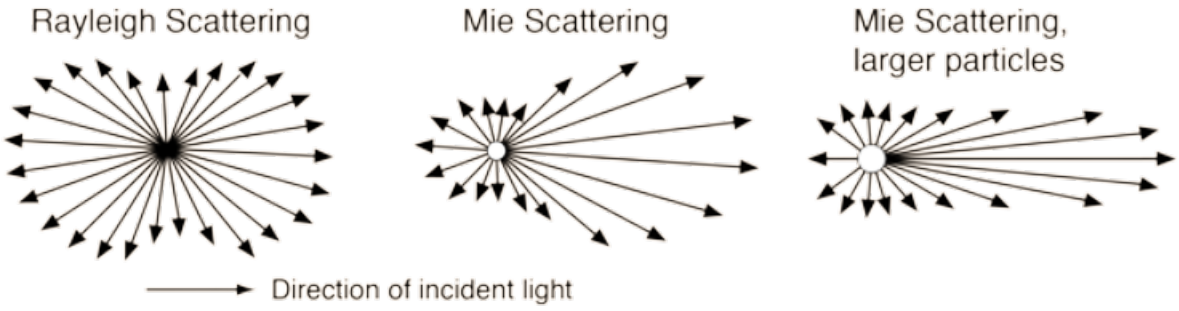

Rayleigh vs Mie scattering intensity lobes [3]

1.1.3 Raman Scattering

Unlike the previous two types of scattering namely Rayleigh and Mie, Raman scattering is an inelastic scattering, which means incident photons interact with the molecules (e.g., in air) in such a way that there is a shift in frequency of the scattered photons across the course of scattering, so that there is energy loss or gain. If the molecules have a higher energy after scattering, it means the scattered photons have lost their energy (Stokes shift). The opposite can also happen if the molecules are initially excited, thus obtaining anti-Stokes components with increased energy. To detail it out a bit, Raman scattering depends on the

polarizability of molecules (so does Rayleigh scattering). For such polarizable molecules, the incident photon with their incident energy excites the vibrational states or modes of the molecule. The amount energy consumed in this results in less energetic scattered photons. If we take a spectrum of these scattered photons, we will be able to get spectral lines below the Rayleigh scattering peak at the incident frequency. These are called the "Stokes Lines".[4]

However, we might also get "Anti-Stokes" spectra lines if the scattered molecules undergo considerable excitation of their excited vibrational states. These comparatively weaker "Anti-Stokes" lines are found at frequencies higher the incident frequency, because they correspond to higher energy, taking into account the fact that the incident photon energy is added to their vibrational energy. Raman Scattering may also involve rotational transition of molecules. Raman Scattering can be observed for molecules without net dipole moment (hence no pure rotational spectra), as it depends on the polarizability of molecules, and they give us information about the moment of inertia and thus the structure of the molecule. Raman Spectra is very precise because it depends on the chemical bonds present in the polarizable molecule and hence are very specific due to these differences in rotational and/or vibrational energies. We are thus able to distinguish the components present in a material from its Raman signal.[5]

But in case the incident photon energy matches the molecule's electronic transition energy, i.e., same frequency, we get resonant signal, the phenomena is known as resonant Raman scattering. In this phenomenon, the molecule after getting to its excited state can either undergo Raman scattering or fluorescence. But usually, the Raman signal is much much smaller, about 10^{14} than fluorescence signal. Thus, in order to analyse the Raman signal, we take help of a process known as Surface Enhanced Raman Scattering (SERS).

1.1.4 Brillouin Scattering

Brillouin scattering[6] is an effect caused by the $\chi(3)$ non-linearity of a medium, specifically by that part of the nonlinearity which is related to acoustic phonons[7].The incident photon changes into a scattered photon and a phonon[8]. The scattered photon is of less energy, propagating in a backward direction, and this loss of energy results in the phonon. Brillouin scattering happens due to the electromagnetic waves coupling coherently with an acoustic or mechanical wave in a light bearing material[9], eg, optical fibre[10] or other optical waveg-

uides. Brllouin scattering can be used for lasing, filtering, sensing and acoustically storing optical pulses. This is because it supplies an extremely narrow tunable line-width response. Brillouin scattering is a complicated interaction and this leads to a number of interesting phenomena:

1. Acoustic mode scattering[11] in a solid[12], where acoustic standing waves are produced according to Bragg's law, scattering incident light waves

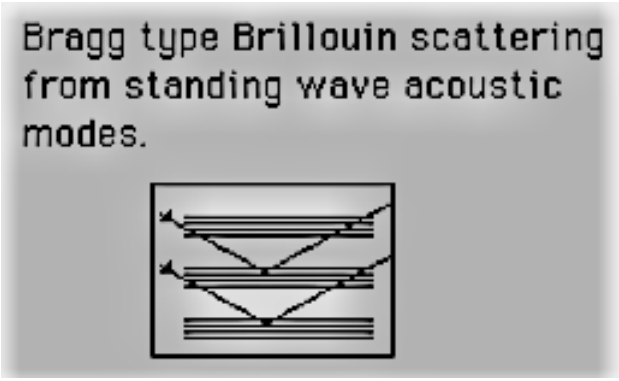

Figure adapted from [8]

2. Acousto-optic modulator, which achieves Q-switching the laser on and off by scattering the incident light from the acoustic waves forming effectie Bragg-type planes, in a quartz crystal[13].

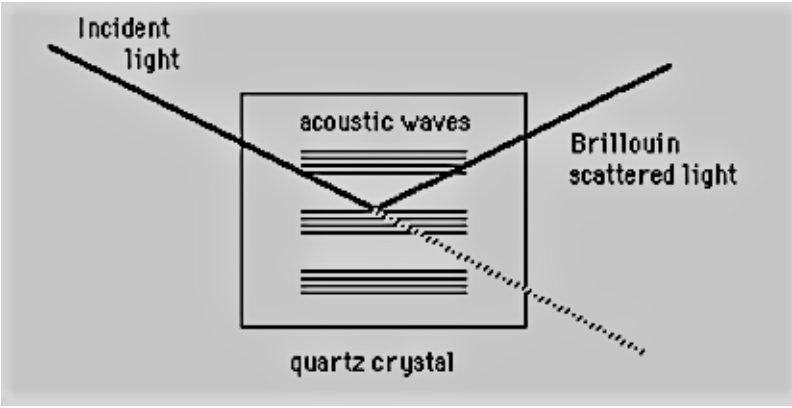

Figure adapted from [8]

3. Laser water scattering, in which He-Ne laser radiation interacting with water leading to side band phenomena[14]

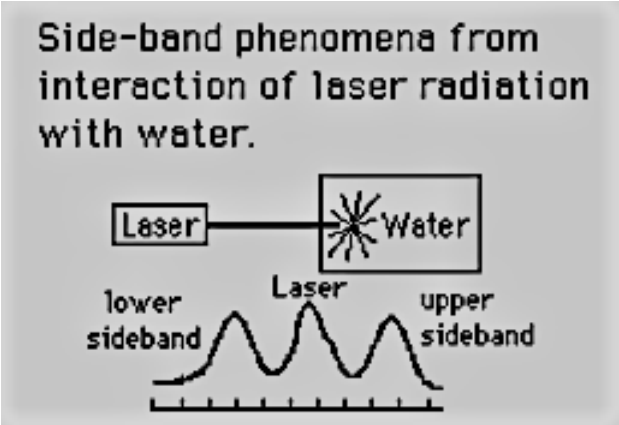

Figure adapted from [8]

1.2. Trapping

Over the years, various kinds of optical traps have been discovered and put into use. It was initially developed by Arthur Ashkin his landmark 1969 and 1986 papers, which we'll discuss ahead a bit. Then eventually, with more research, much more efficient optical tweezers were developed for trapping not only big dielectric particles in liquids and gases but also diffraction limited nanoparticles, from both metal-dielectric interface and not just trapping them but also controlling and manipulating them. What's even more impressive is that these tiny nanoparticles, beyond the scope of imaging of most microscopes can only be trapped and manipulated on surface but in bulk as well, with enough power and proper efficient techniques.

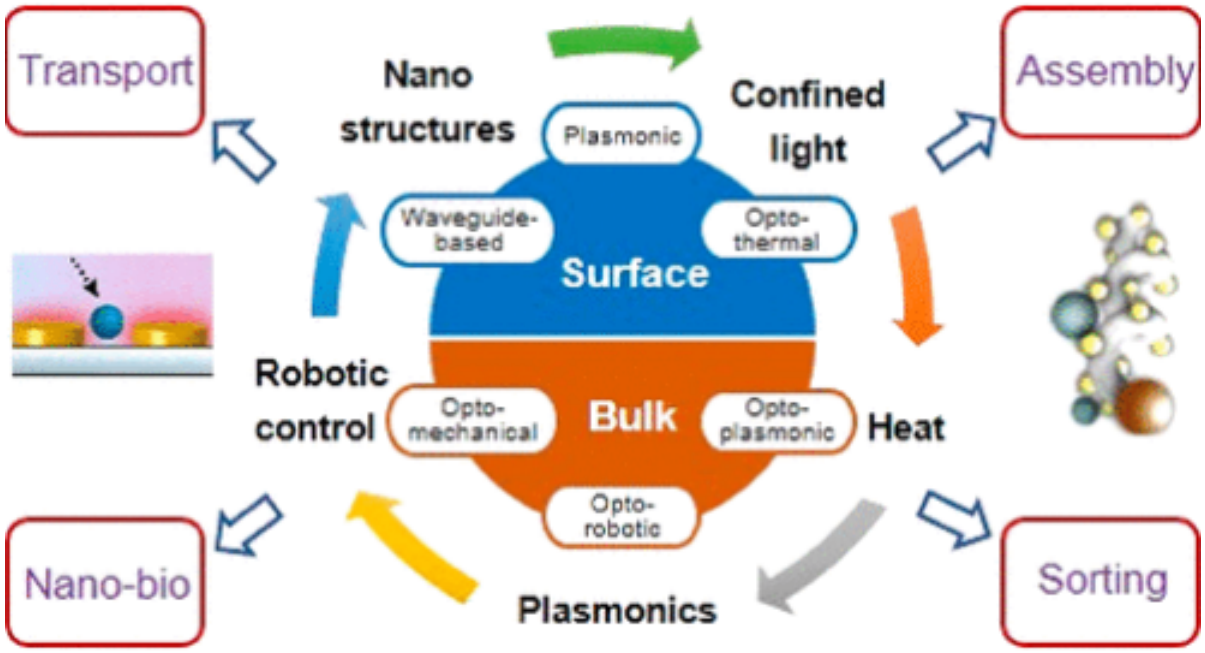

Figure adapted from [15]

We'll see some of these different developments now to get an idea.

1.2.1 Simple Optical Trapping

In 1969, Ashkin[1] et al reported observations of accelerating and trapping particles of the order of microns, freely suspended in liquid and gas, with just the radiation pressure from a continuous laser. This was historic because it hadn't been observed before and this lay the foundation stone for optical tweezers. The pressure forces created a potential well, which put an inward force on the spherical molecules. Sixteen years later, he successfully created the first optical tweezer[16] and demonstrated the trapping and manipulation of microorganisms like bacteria and viruses, thus not just spherical dielectric particles but living matter as well. A three-dimensional trap was demonstrated and their manipulation was shown. Ashkin even showed that they maintained their normal behaviour, both inside the traps, and outside too, when the laser was turned off.

To detail the working a bit, basically what happens is the laser beam used for trapping is tightly focussed at the beam waist and this is the region where the particles or microorganism, whatever region they may belong to (Mie or Rayleigh), get trapped[17]. The working force is the strong electric field gradient. The dielectric particles are attracted towards it and don't move much from the centre of the beam waist. the concept being somewhat similar to Hooke's law. However, the exact equations applicable depend on the relative size of the particle to be trapped and the wavelength of the laser light used, where if the two dimensions are comparable, then Maxwell's equations along with proper boundary conditions must be used, in order to give the system an accurate treatment. Thus, the trapping mechanisms differ according to whether the order of the size of the trapped particle/microorganism is larger than the wavelength of the trapping laser used (Mie region) or it is smaller (Rayleigh region).

1.2.2 Optothermophoretic Trapping

Optothermo-electric nanotweezers (OTENT)[18] uses the laser indirectly to create a thermally induced electric field in an ion solution, which counters the Brownian motion directed away from the beam focus, thus keeping the trapped dielectric particles in place. The main advantage of this method is that we are not only able to trap and manipulate nanoparticles, that too in a solution, in the presence of strong diffusive Brownian forces, but also bigger colloidal particles, which would get more heated due to increased cross-section and hence stronger diffusive force, that too at a much lower laser power, almost three orders less than that required in conventional optical trapping. This was first shown by Zheng et. al.[2]

Thermophoresis is the trick which helps us cutdown on the excessive laser power. Prior to this method, on trapping subwavelength nanoparticles, the trap stiffness would have been reduced, and hence more laser power would have had to be applied. Although Au and Ag nanoparticles would be trapped successfully, localized surface plasmon excitation at the metal nanoparticles by the laser would lead to increased absorption and scattering. Hence the particles would get heated under the strong optical force of the incident focussed laser beam, thus making the trap unstable. Thus, the trap wouldn't be so efficient and even ran the risk of damaging the properties of the particles to be trapped, thus defeating the purpose of the experiment. However, now it has been mitigated. The directed motion

of an object (here particle), in reponse to the applied temperature gradient is referred to as thermophoresis or the Soret effect. The drift velocities (u) of particles subjected to the temperature difference, in the solution, is given as

$$u = -D_T \nabla T$$

where ∇T is the temperature gradient and D_T is the thermophoretic mobility.

The steady state concentration gradient is given by

$$\nabla c = -c\frac{D_T}{D}\nabla T = -cS_T\nabla T$$

where c is the concentration of the solutes, D is the Brownian coefficient, and $S_T = \frac{D_T}{D}$ is the Soret coefficient. A *positive* value of the Soret coefficient implies *thermophobic* behaviour whereas a *negative* value implies *thermophilic* behaviour.

When a temperature gradient is applied across an electrolytic solution, the charged ions migrate according to their respective charges, due to thermophoresis, setting up a thermoelectric current. Now, owing to different Soret coefficients and physical properties of the ions e.g. charge, solvation energy and ionic radius, they migrate at different drift velocities. The charge characteristic determine if they will drift towards the hotter or colder region. This Seeback effect observed in the thermoelectric field set up by the application of temperature gradient is given by

$$E_T = \frac{k_B T \nabla T}{e}\frac{\sum_i Z_i n_i S_{Ti}}{\sum_i Z_i^2 n_i}$$

where k_B is the Boltzman constant, e is the elemental charge, T is the ambient temperature, i is the ionic species, and n_i,Z_i and S_{Ti} are the concentration, charge number and the Soret coefficient of the ionic species respectively.

Mechanism of CTAC

To make the solution ionic, in order the thermoelectricity to get set up, the cationic solvent CTAC (cetyltrimethylammonium chloride) as added to the colloidal solution of metal nanoparticles. On dissolving, a double molecular layer of positive charge is formed due to

adsorption of CTAC molecules on the nanoparticle.The CTAC concentration needs to be above a Critical Micellar concentration(CMC) for the CTAC to self assemble into macrocations. When no laser is applied, the nanoparticles and CMC ions are distributed in the colloidal solution. Also the solution is put on a thermoplasmonic structure, in this case a porous gold coated glass side. However on application of the laser, the gold heats up and a temperature difference of approximately 12K at the gold surface – solution interface is enough to set up a thermoelectric field. Now both the positively charged micellar macrocations and the Cl- anions undergo thermophoresis and migrate from hot to cold region, but their relative drift velocities are much different. The molecular mass and Soret coefficient is much higher for CTAC micelles than the chloride anion. Thus, the CTAC micelles drift away to the surrounding colder region faster than the Cl- ions. Thus, a Thermoelectric current is set up directed towards the heated laser spot, from the positive ctac micelles to the chloride ions. This field counters the repulsive and diffusive forces of the optically heated nanoparticles directed away from the heated region, and holds the nanoparticles in place, under the focussed laser illumination. Thus the OTENT trap is formed[18]

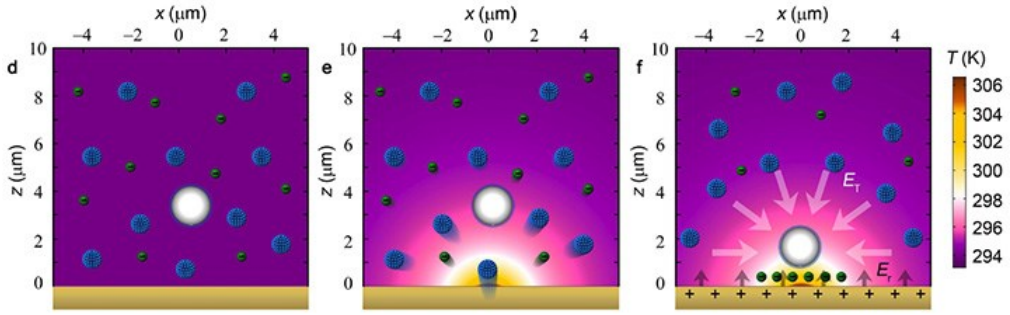

Before laser heating (left), positive and negative ions are evenly distributed. Laser heating causes differential migration of ions in the suspension (middle), creating electric field that traps the positively charged nanoparticle (right)[Image: Courtesy of Linhan Lin[18]]

1.3. Introduction to Differential Dynamic Microscopy

To infer particle dynamics in soft matter physics, there have been many techniques developed over the years . Some of them are multiple particle tracking subroutines by David Grier

originally in IDL, later adapted into MATLAB subroutines and latest in being python as well , fluorescence correlation spectroscopy studies, particle imaging velocimetry (commonly known as PIV), diffusing wave spectroscopy and photon correlation spectroscopy (commonly know as Dynamic Light Scattering or DLS). These techniques are used according to their pros and cons, considering which process will be better fit in the particular experiment concerned.[19]

Prticle tracking methods serve better when the sample is less dense and we want to focus our study on individual particles, its trajectories and and veocity and other characteristics. for PIV methods we need to have tracer particles which themselves won't have any effect on the system as a whole but will help us to find out about the larger particles in the system concerned in a microrheology soft matter sample. Dynamic Light Scattering methods on the other hand look at the ensemble behaviour statistics across multiple length-scales. A collimated source of light is directed towards the sample, and fluctuations of the scattered light is measured as it passes through the smple. Now these fluctuations are correlated over the entire sample space with varying θ and dynamics of the scatterers present in the sample extracted.

But these particle tracking and dynamic scattering techniques are not very efficient if the sample is very dense with many scatterers. This where DDM (differential dynamic microscopy)[20][19] comes in and saves us. Specially for samples which have weak scatterers or are very concentrated and dense, or there is less ssample volume, DDM works like a charm. It doesn't even need a very sophisticated microscope set-up and the sample on which this digital microcopy using Fourier techniques will be run and analysed need not be homogenic,i.e., it can have scatterers which have different different decay constants, eg. plasmonic nanorods have considerably different translational and rotational diffusion coefficients and ddm will still be able to capture these dynamics.

Now we need to discuss on exactly why using a digital Fourier microscopy technique and why they are so advantageous. Soft matter dynamics can be equivalently both in real space and reciprocal space. Now conventionally people preferred using the real space techniques because they could be tracked unambiguously [21] using far-field scattering techniques. However there is increasing difficulty to study theri dynamics as we increase their concentration ans also as the particle size decreases and approaches diffraction-limited length-scales. Equivalently, the near field scattering data can be Fourier transformed and studied in the reciprocal

space, allowing us a lot of liberty in the previous problems and also whilst conserving information. If the dynamics being studied in real-space is described by linear PDEs, then these partial differentials can be transformed to their corresponding algebraic equations in the reciprocal space, thus making the eigenmodes of the system accessible.[21][22] [23]This leads to reciprocal space techniques being favoured in matters of tracking particles in real-space.

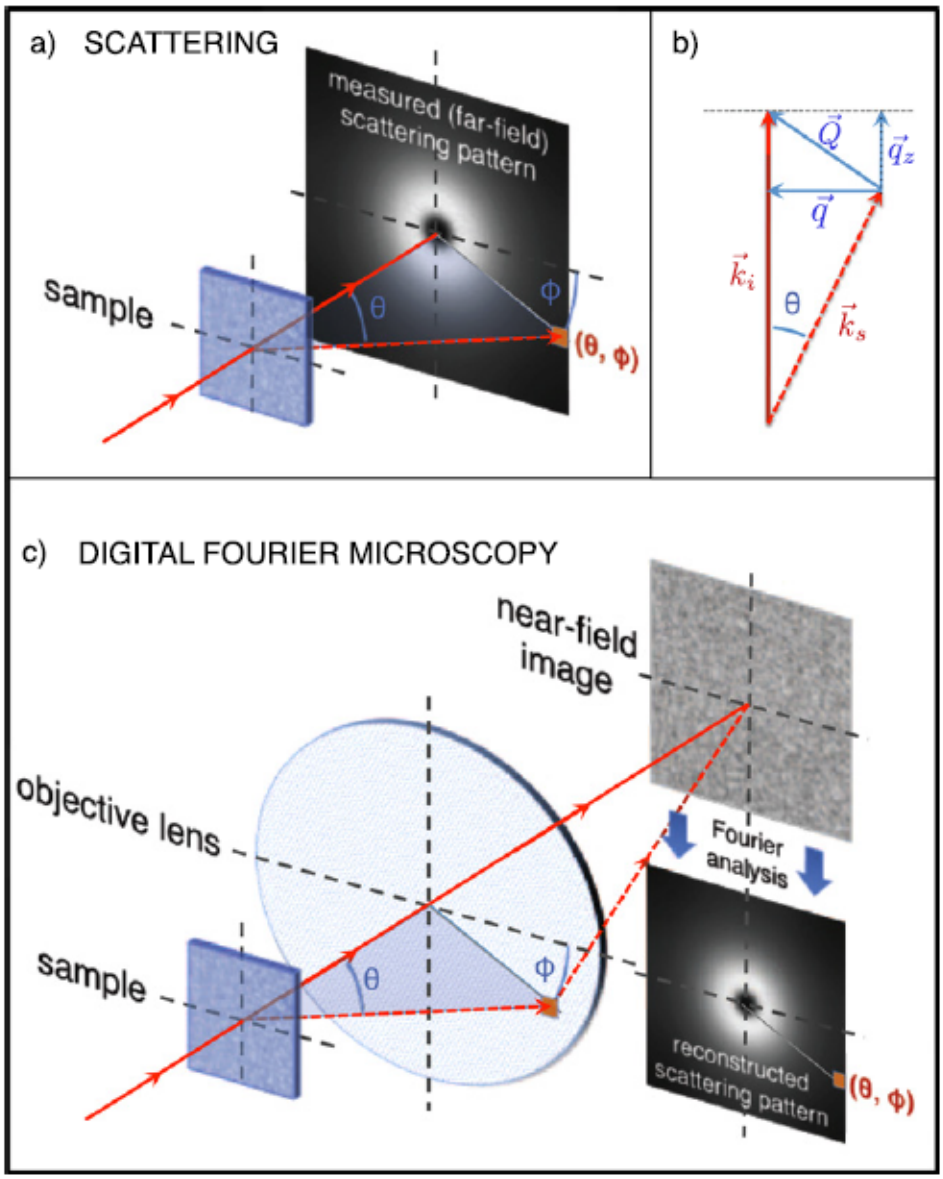

a-scattering experiment data collection, b-Wavevectors involved in the scattering process, and c-Sketch of a digital Fourier microscopy experiment Image adapted from [21]

In a traditional far-field experiment, after scattering the scattering wavevector can be defined in terms of a plane wave traveling with wave-vector k_s such that $\mathbf{Q} = \mathbf{k}_i - \mathbf{k}_s$. The scattered ray can be defined in terms of polar angle θ and an azimuthal angle ϕ, which corresponds to a point described by (θ, ϕ), in the scattering far-field pattern. In the DFM experiment, equivalent information can be collected from the near-field scattering data by Fourier transforming them, isolating the scattered ray and collecting its data based on the 2D projection of q on Q during the scattering process.[21]

In DDM, initially the difference of images are taken. By this, we mean the intensity differences.

$$D\left(\mathbf{x}, t_0, \Delta t\right) = I\left(\mathbf{x}, t_0, \Delta t\right) - I\left(\mathbf{x}, t_0\right)$$

Now this x is replaced by q which considering the sample to be radially symmetric, where

$$q = \sqrt{x^2 + y^2}$$

Thus D is essentially nothing but

$$D(\mathbf{q}, \Delta t) \equiv \left\langle |\Delta \hat{I}(\mathbf{q}, \Delta t)|^2 \right\rangle$$

It is just the expectation value of the Fourier power spectrum of the image intensity differences.[19]

Next Giavazzi et al [24] showed that in LSI model of microscopy, the dynamic structure function analytically decompose to essentially 3 sub-functions:

$$D(\mathbf{q}, \Delta t) = A(\mathbf{q})[1 - g(\mathbf{q}, \Delta t)] + B(\mathbf{q})$$

Bayles[19] used it and showed that similar derivations follow in dark field as well, i.e. in LSV models. She also showed that ddm data when applied on dark field gives us much less noise and better results. We have followed the same here. A(q) cooresponds to optical functiona and depends on our optical system, b(q) is just the noise from these. As long as we have A(q) greater than B(q), we are good.

Here, in our case, the intensity autocorrelation function is

$$g(q, \Delta t) = e^{-\Delta t/\tau(q)}$$

with $-\Delta t$ being the time difference and τ(q) being the relaxation time period.

Chapter 2

Preparation of Plasmonic Structures

2.1. Preparation of Gold Nanoparticle

For preparing gold nanoparticles, we followed the process given by given by Lee and Meisel in this paper[25]

1. 480 mg of $HAuCl_4$ was taken and put in 1000 mL water.
2. The solution was then stirred and heating was started.
3. After the solution was brought to boiling, 100 mL of 1% sodium citrate solution was added to it.
4. The resulting solution was boiled for approximately an hour.
5. The final solution was wine-red in colour.

2.2. Preparation of Silver Nanoparticle

For preparing silver nanoparticles also, we followed the process given by given by Lee and Meisel in this paper.[25]

1. 180 mg $AgNO_3$ was dissolved in 1000 mL of water.

2. After stirring, the solution was put to heating.

3. After the solution was brought to boiling, 20ml of 1% sodium citrate solution was added to it.

4. The resulting solution was boiled for approximately an hour.

5. The final solution was greenish-yellow in colour.

6. Samples from the final solution were then centrifuged with acetone and later ethanol to clean the wash the particles off residues. The residual solvents were then decanted and the dense solution of cleaned silver nanoparticles were stored, away from light.

2.3. Preparation of Gold Nanoplate

For preparing gold nanoplates, we followed the process given by given by Kan, Zhu and Wang in this paper.[26]

1. 1 0.2M solution of HAuCl4 was prepared and 1ml of it was added to 6 mL ethylene glycol.

2. The solution was slowly stirred in a round-bottom flask, with the temperature being maintained at around 150 °C . A thermometer was equipped with the setup for this purpose.

3. Then 3 mL ethylene glycol solution of poly(vinylpyrrolidone) (PVP 222 mg/mL, Mol. wt. 40,000) was injected dropwise.

4. After around 10-15 minutes, shiny objects were detected inside the beaker.

5. The reaction mixture was continuously heated and stirred for about 30 minutes, with increasing number of shiny products (as more and more gold saturated in the form of nanoplates)

6. Ethylene glycol has a high boiling temperature (198 °C). This coupled with the gelation property of PVP has a negative effect on the following characterization. Hence, Hence the samples were collected at different times from the mixture to ensure the collection of optimum gold nanoplates.

7. Eventually, the resulting mixture was cooled off and extracted with acetone.

8. After proper centrifugation, the remaining solvent containing residues were decanted off and the fresh gold nanoplate solution was stored, after a few more rounds of centrifugation with deionized water to clean them off.

9. Around 5 micron gold plates were obtained. Some hexagons were obtained too.

Chapter 3

Experiment And its Results

This section details everything regarding the experiment, all the procedures and analysis that was done.

3.1. Experimental setup

A 633 nm laser and a 532 nm laser was used to trap the sample. They were directed to the microscope through a periscope, and from the microscope, images were captured in an EMCCD. 2 mirrors were use, one being flip, in order to alternate between the 2 lasers and compare their trapping efficiencies. The 532nm laser has a power of 30 mW and an effective power of 7mW, while the 633 laser has a power of 25 mW and an effective power of about 3.5 mW. Power is measured immediately coming from the laser, and effective power refers to the power at sample plane after passing through all the optical elements on its optical path. However, the 633 nm laser is slightly more effective in trapping the nanoparticles, although proper CTAC concentration regulation gave effective traps on both lasers. A schematic of the experimental setup is given here.

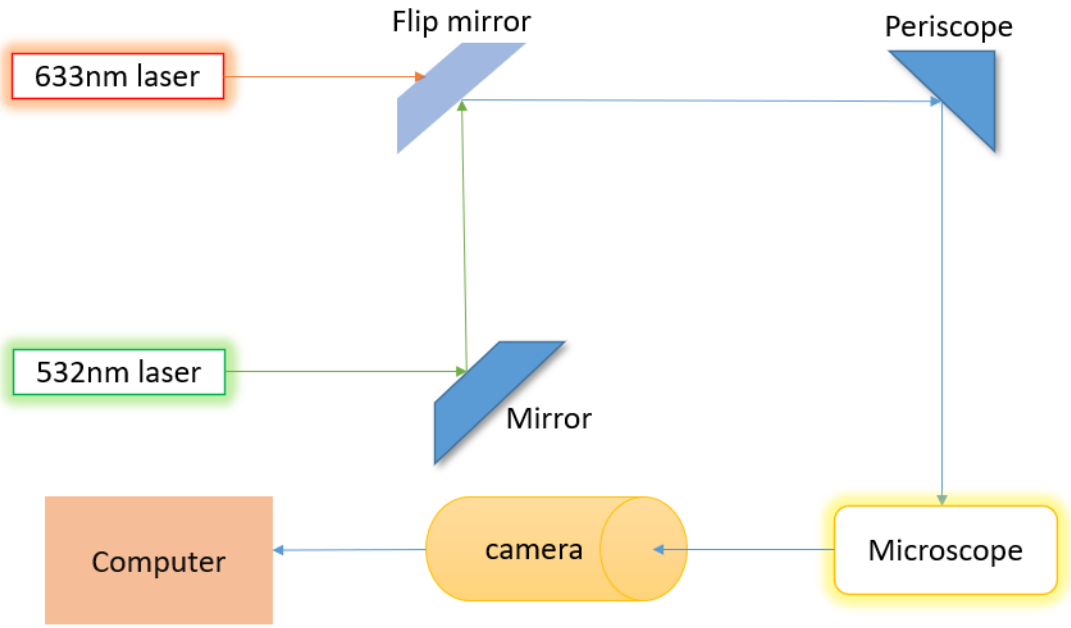

A schematic diagram of the experimental setup

3.2. Experimental method

3.2.1 Preparing the samples

Like any other experiments, over time a lot of things need to be tried out and many adjustments need to be made in order to get the most efficient setup that gives us the best results. Multiple samples were observed and the optimum concentrations and optimum objective lenses were used in order balance the trade off between higher contrast and magnification to observe the super tiny Au and Ag nanoparticles both individually and in clusters.

1. A chamber was taken and stuck on a substrate. The subtrate were of two types:
   (a) a glass coverslip
   (b) a 10 nm Au film coated on one side of a glass coverslip

2. An 8 μl solution of 400 nm Ag nanowires in ethanol was dropcasted on the substrate of the required type.

3. It was allowed to dry so that the silver nanowires stuck to the substrate and not get displaced on putting the water-based sample on top of it.

4. Then a 16 μl colloidal solution of 250 nm Au nanoparticles in water was dropcasted over the substrate.

5. The chamber was closed off on top with a glass slide to reduce the rate of evaporation and preserve the sample for later usage.

Note: We also used glass slide on one side instead of a glass coverslip so that the sample becomes more robust. The glass cover-slip may be so thin that during darkfield observation, it may bend due to pressure from the condenser lens and not only bend and distort our readings but also break and damage both our sample and microscope. The glass slide on one side also makes the sample sturdy and robust enough to carry it around. A schematic of the the sample slide is shown.

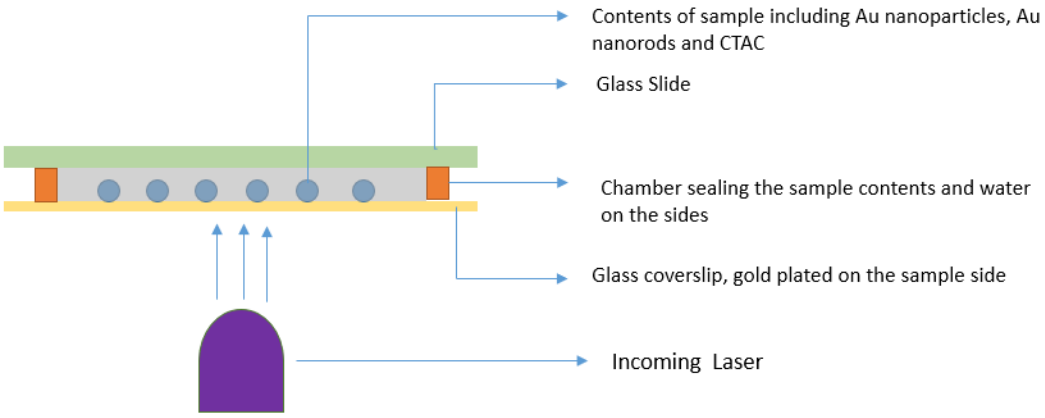

A illustrative diagram depicting the way samples were prepared and kept on the microscope stage

3.2.2 Performing the Experiment

Our trapping experiments were conducted in dark field. For getting a good dark field image with proper contrast, 1.4 NA oil condenser was used and 100x 0.8 NA air objective lens was used. Both 533nm and 633nm wavelength lasers were used for excitation, delivering a power of about 7 mW and 3.5mW respectively.

We conducted a step by step otent experiment from the very basic, so that we are able to understand the effect every component in the sample has on the dynamics of the nanoparticles, be it the nanorods or the laser or the ctac.

1. So first we observed pure brownian diffusion for just nanoparticles.
2. In the next sample, we dropcasted the nanowires first, then added the nanoparticles, and just observed them.
3. Another sample was prepared having the same exact contents, except that CTAC was added (more than the CMC concentration of course).
4. Other 2 samples were prepared in the same exact process (with and without CTAC), but just on glass coverslip,i.e., without gold film coating.
5. Then these were illuminated with both lasers, one by one. These dynamics were recorded with 17 fps for ddm analysis.

	-ctac -film	+ctac -film	-ctac +film	+ctac +film
532 nm	A1	B1	C1	D1
633 nm	A2	B2	C2	D2

Different samples prepared

3.3. Observations and Results

We observe that there is only partice agglomeration in the final combination of ctac + gold film sample. Other samples did not give such a OTENT strong trap as this one. We try to classify these processes with the ones we already know namely, ballistic, super-diffusive, diffusive, sub-diffusive and confined motion, by plotting their diffusion graphs against spatial wavevectors and time.

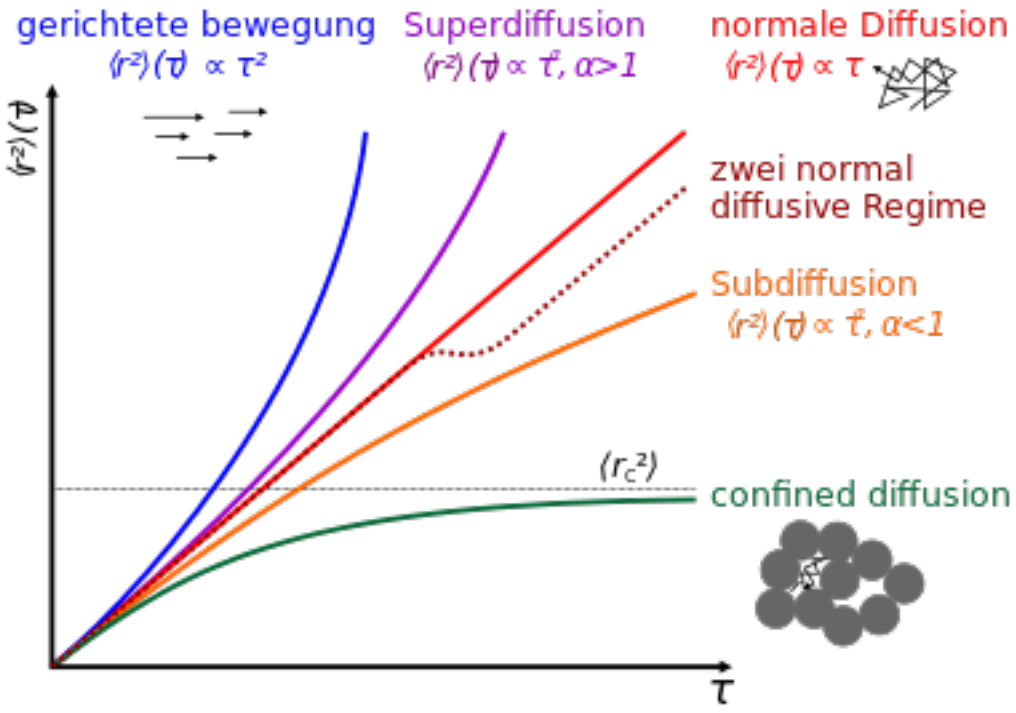

Vrious Diffusion processes according to their mean displacements relative to timescale [Source: Wikipedia commons]

	-ctac -film	+ctac -film	-ctac +film	+ctac +film
532 nm	No aggregation	No aggregation	No aggregation	Aggregation attained
633 nm	No aggregation	No aggregation	No aggregation	Aggregation attained

Corresponding observations

We will come to data after presenting some initial data on some experimental records we had taken in order to verify and cover our bases. As a form of control, we ran the ddm processing on the data collected from a sample of 3 micron silica beads in water.

The processed image is attached herewith.

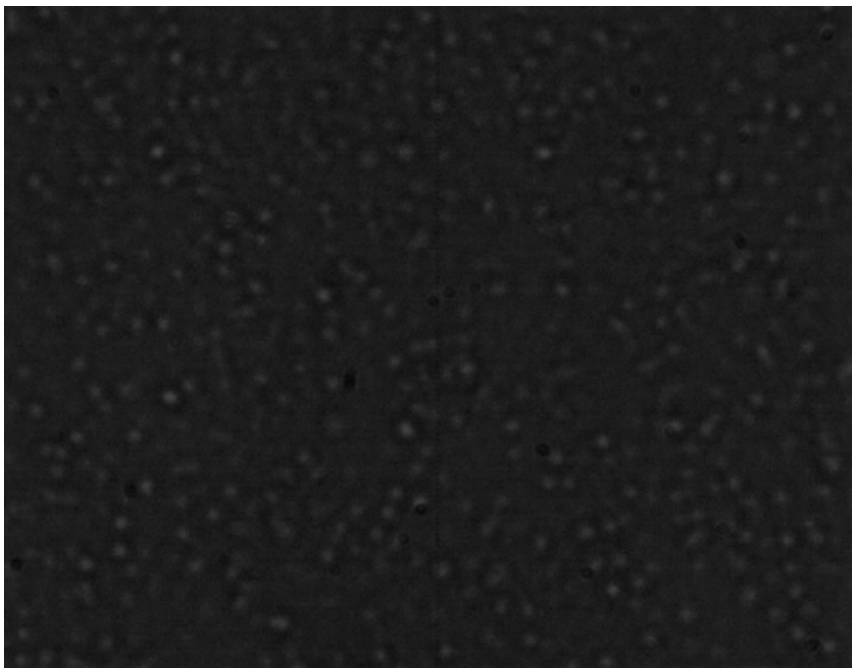

3 micron Silica beads

When we take diffences of subsequent images, separated in time, we tend to retain the

sharp edges and differences. In this case, the residual information pertains to the change in the sample, i.e. particles shifting slightly from their position due to the various forces acting in the system. Now when we take a Fourier transform of them, we preserve information both in frequency(time dimension) and wavevector space (spatial dimention). A typical Fourier transform of the difference image looks like this.

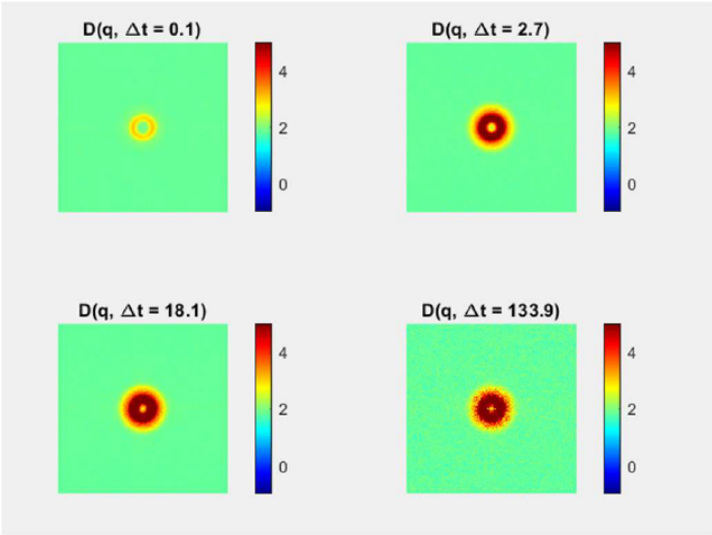

Image structure function as a function of q for selected t (This is the radial average Fourier power spectrum of the difference images)

Then we plot the dynamic image structure function D(q,$\triangle$ t), which is our mean power spectrum of the image intensity difference (defined in ddm theory section), with q. since it is a function of our wavevector q and time difference $\triangle$ t. We can choose any specific time-difference for our plotting. We can see that as we move up the graph the specific $\triangle$ t increases from around 0 to 134 seconds, taken at regular exponential intervals.

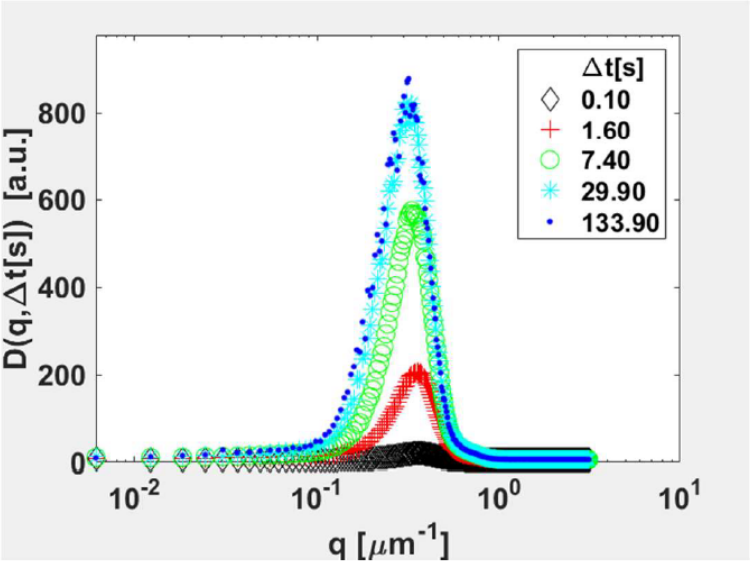

This is the graph of the image structure function vs wavevectors for various time intervals. The trend is that the time intervals decrease from top to bottom of the Gaussian(along the y axis)

we finally have the graph for τ vs q, and from its slope we get the diffusion constant from the equation

$$\tau = \frac{1}{D^2 q}$$

, where tau is the relaxation time,q is the wavevector and D is the diffusion constant. We found this to be around $1.2 \times 10^{-4} \mu m^2/s$.

Now we can cross-check this with conventional Stokes-Einstein Equation,

$$F = \frac{k_b T}{6\pi\eta r}$$

, where k_b is the Boltzmann constant, taking the value of $1.38064852 \times 10^{-23}$ m^2 kg s^{-2} K^{-1}, T is the temperature of the medium, being taken as 293 K , η is the viscosity of medium, here water, being 1.002 Pa-s and r is the radius of particle which here is 1.5 micron.

This formula gives us a value of $1.43 \times 10^{-4} \mu m^2/s$, which is pretty close. The concentration was around 30 % w/w.

		value	units	link	description
D	=	**1.42787679729e-16**	**m^2/s**		**Diffusion coefficient (dimensionless)**
T	=	293	K		The temperature (dimensionless)
n	=	1.002	Pa*s		The dynamic viscosity (dimensionless)
r	=	1.5	micron		The radius of the spherical practicle (dimensionless)

For ddm of our experiments, we used the MATLAB codes of DDMCalc.[19]

Now we move on to the actual experiment.

We have taken tiff sequence of the videos of the otent trap recorded and then spatially segmented it into different tiff stacks. The include 4 regions,

1. a reion with a single particle diffusing

2. a region containing just the trap, i.e., particles coming into the trap and staying there

3. a region near the trap from which the particles are attracted to the trap

4. the entire frame itself, containing all the above elements.

3.3.1 Normal Diffusion Segment

This is the portion where we have just diffusion with particles much farther away from the laser spot or the otent trap site. The diffusion graph is included here. The others are not because they are pretty similar to the earlier diffusion graphs.

We also received this kind of pure diffusive motion when the laser was off initially.

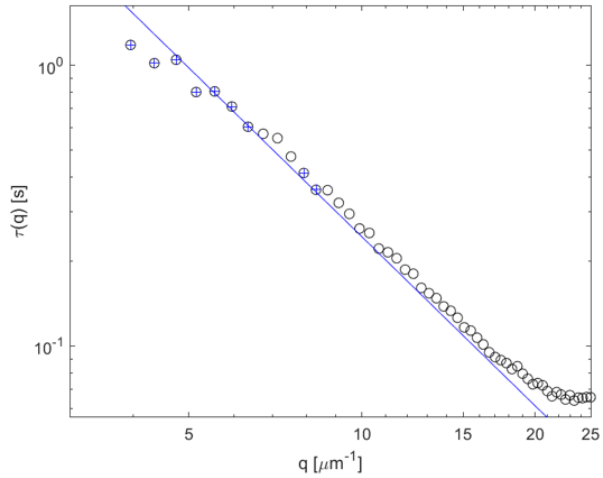

Diffusive motion much away from the influence of laser

The coefficient of diffusion obtained from the slope was about 0.002 $\mu m^2/s$.

Comparing it against the Einstein-Stokes equation gives us about $1.7 \times 10^{-3} \mu m^2/s$

		value	units	link	description
D	=	**1.71345215675e-15**	**m^2/s**		**Diffusion coefficient (dimensionless)**
T	=	293	K		The temperature (dimensionless)
n	=	1.002	Pa*s		The dynamic viscosity (dimensionless)
r	=	.125	micron		The radius of the spherical practicle (dimensionless)

3.3.2 Super Diffusion Segment

This a region from which the laser is at a distance, but near enough to attract particles from here. In fct, the sttractive force of the trap gives them momentum so fast that they go from diffusive motion to a super diffusive motion with a constant of $0.06 \mu m^2/s$. A seperate transiton image is not shown because there are always more particles to replace the old partcles of this region, who are now going towards the trap. So unless quantified, it was not

clear to the bare eye, since this is sort of a transition region. However the diffusion graph is included.

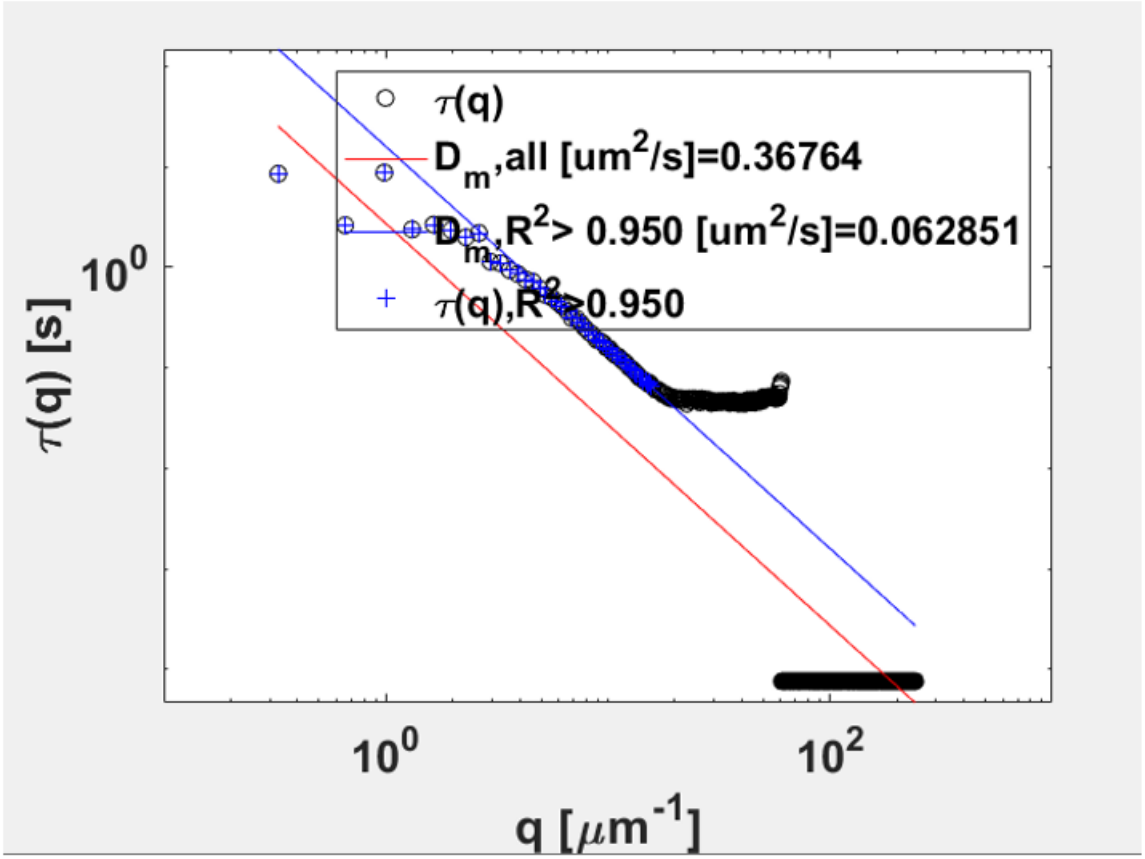

Fast motion of particles approaching towards trap.

The Fourier difference image is also included so that we get to understand the sharp changes in the trajectories of the existing particles, and also their changing number, leading to more and more accumulated difference.

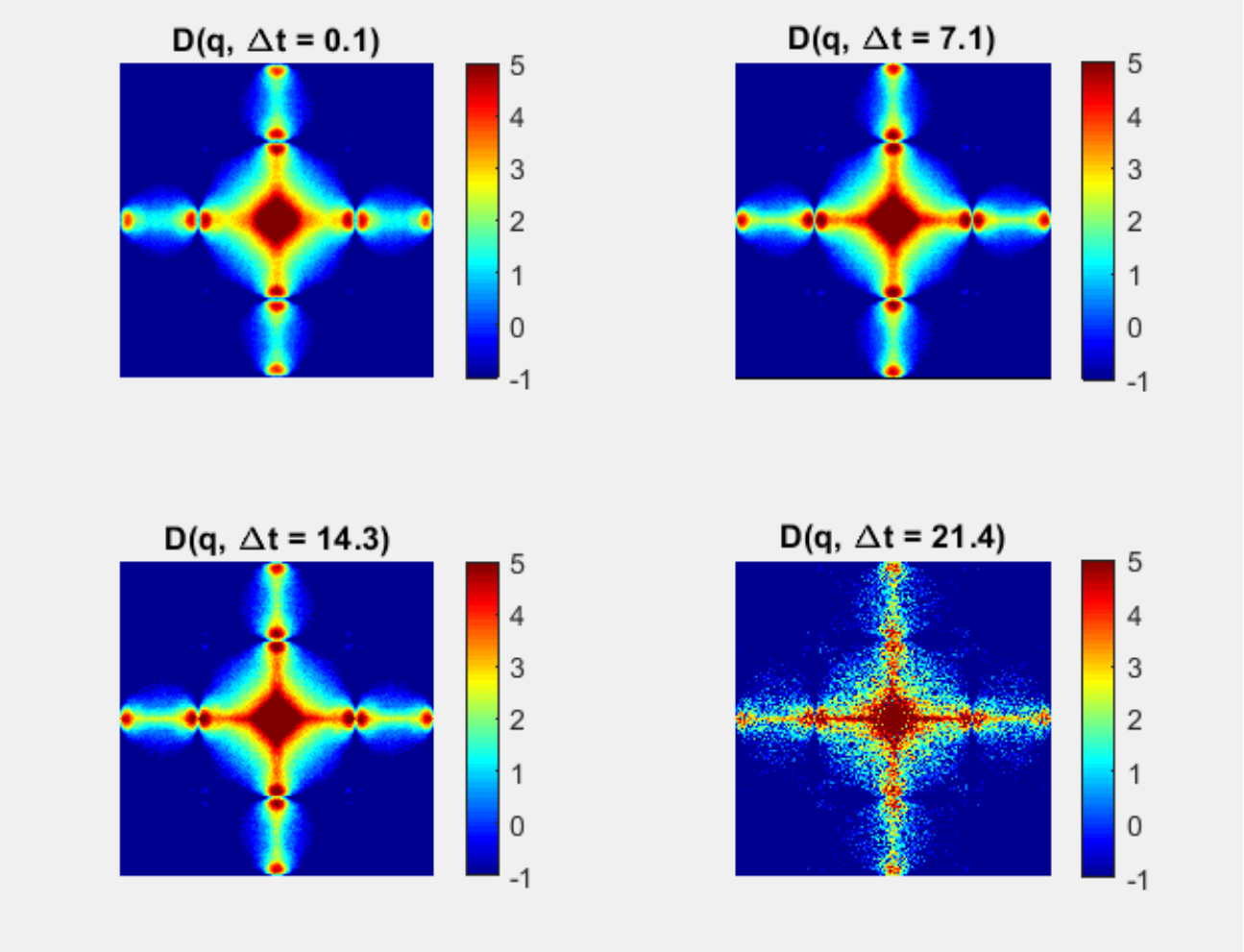

Fourier transform of difference images, highlighting the sharp changes in intensity in the sample region and its underlying cause due to the undergoing activity .

3.3.3 Trapping Segment

This just includes the trapping segment of the frame. Very little margins were left while cropping the trap, as can be seen in the image provide here, because if too much of the trajectories of the particles were included, then that could alter our study of motion in the trap. Basically we were interested to know in the motion which is undergone inside the trap.

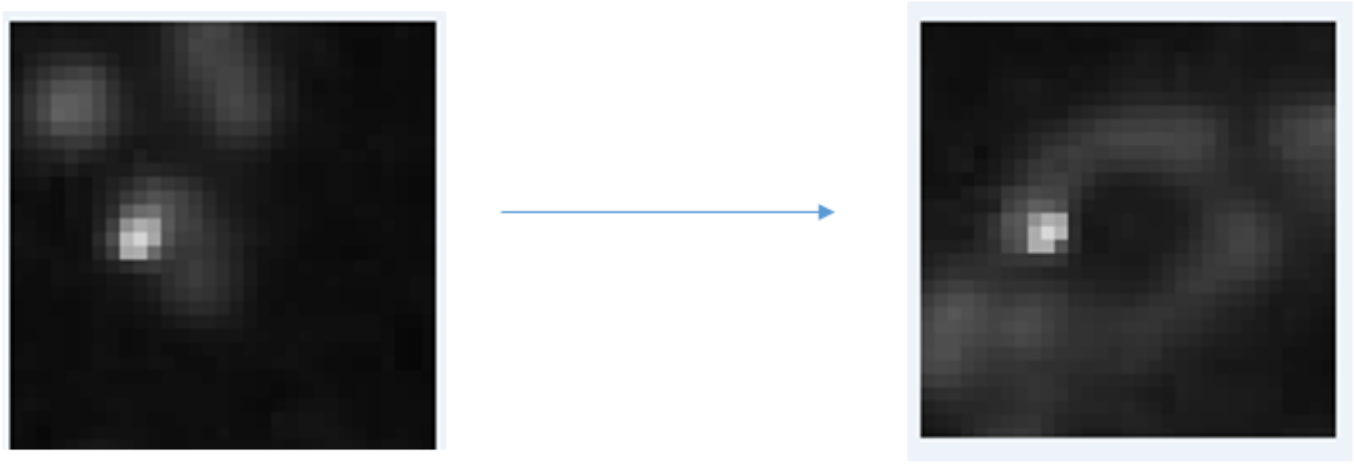

This shows the transition of tiff stack images from the starting of the trap to the end, when we turn off the laser after keeping the particles there for about 100 seconds.

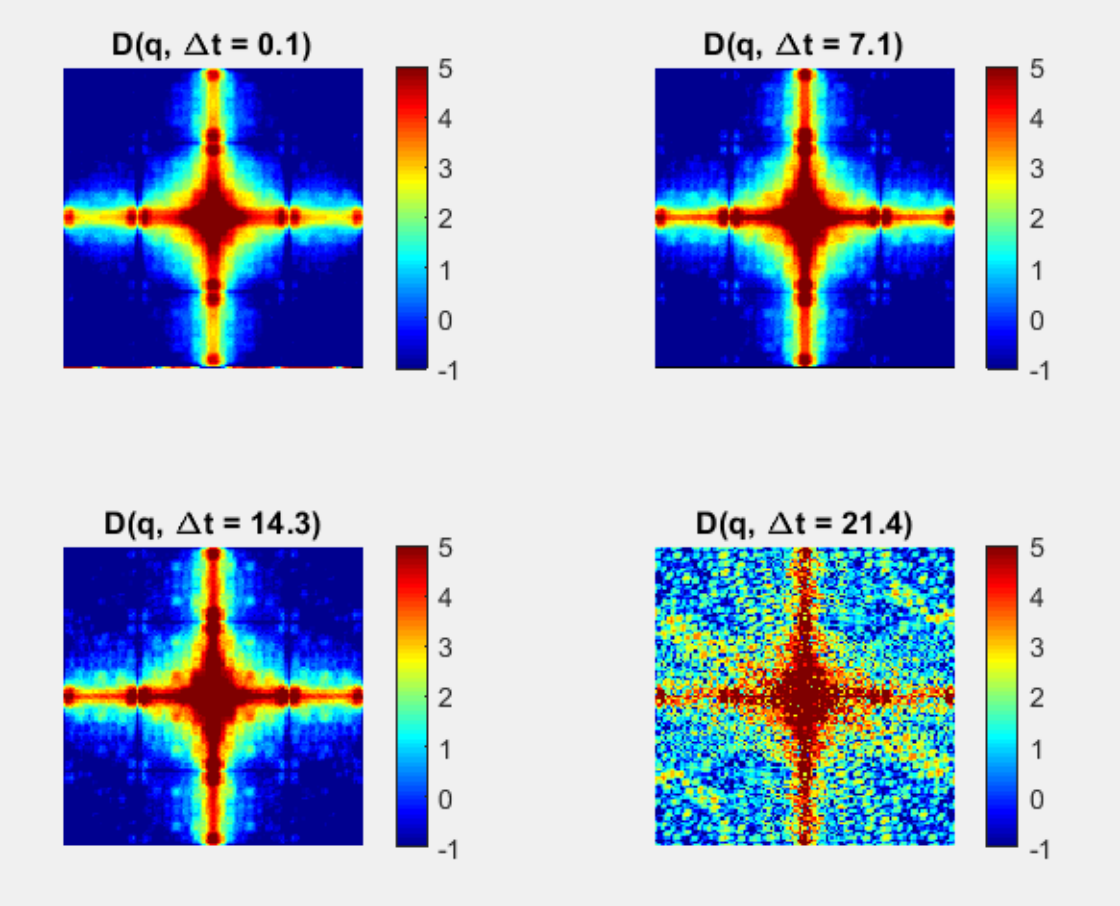

Fourier transform of difference image of traps. We can see because of the sheer density of particles and the trap's rotational motion, how different this FT diagram looks like than the others

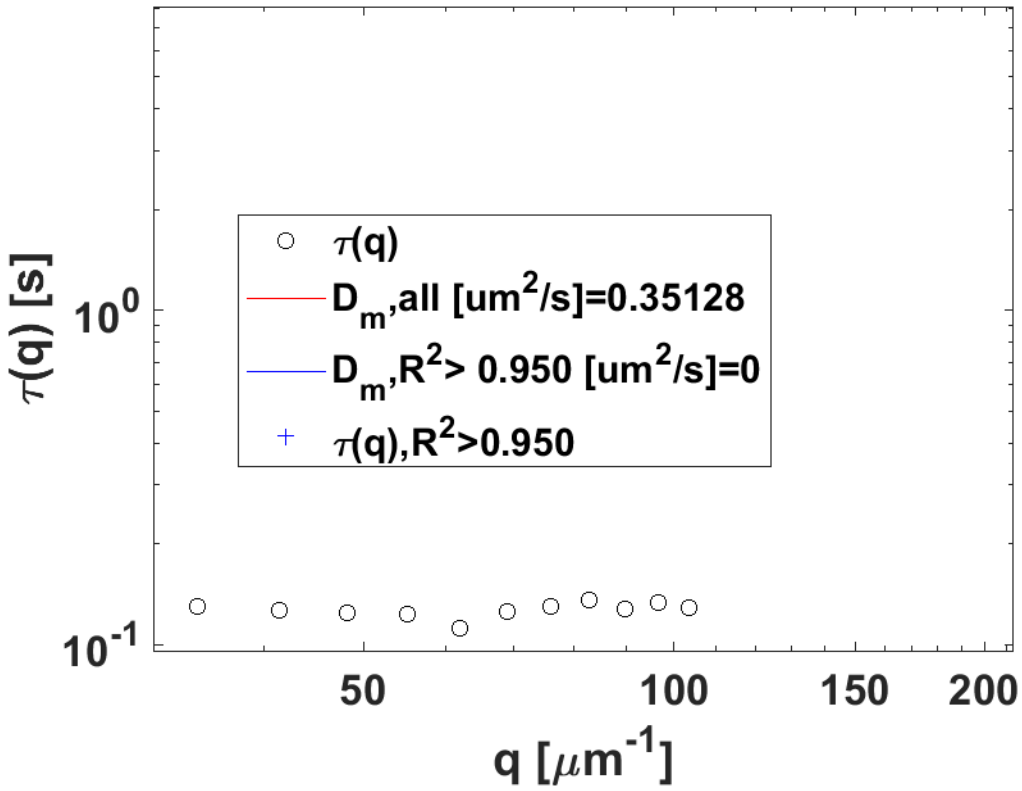

Very confined motion in trap.On plotting the equation from the data points, we get almost a line with zero slope. Also, the D_m having 95% confidence gives no diffusion value, i.e zero.

We can see that the diffusion constant from data within the confidence interval barely have a slope and they barely have their individual motion. Mostly the trap has some sort of rotational motion from all the particles coming in and bombarding but that's it.

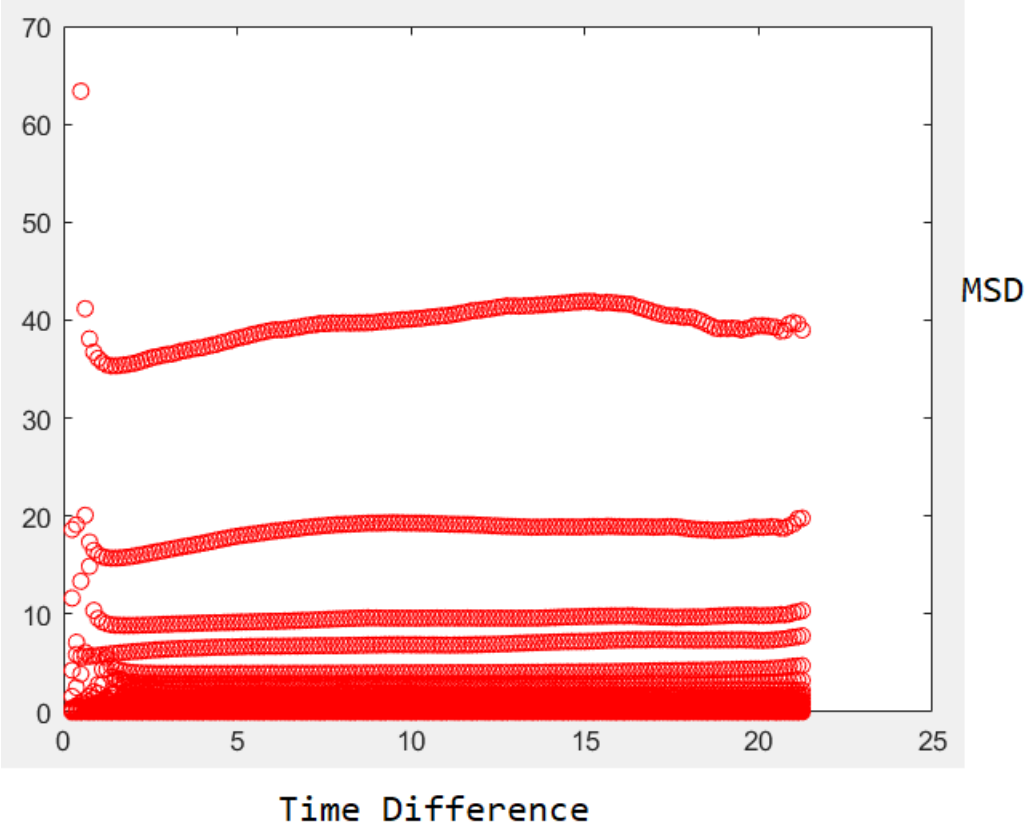

MSD vs time difference graph

We can see here that the graph has almost no slope. The y axis is the MSD and the x axis is the time difference. The trap is so compact that there is no space inside the trap for the particles to move in it.

3.3.4 Entire Video

Apart from analyzing these motions individually, we also wanted to see if we could figure out anything interesting on analyzing the entire frame with all these various diffusive processes as a whole in one go. From the results, we see that that the superdiffusive motion was the most prominent one, with particles coming into the trap. However there were various order of diffusion presumably, due to the varying forces throughout the sample space. They were however not quantified this time, since it was already done separately before. also since there are all the processes happening from sub diffusion to super diffusion and even no motion in

the trap, we should probably take the overall diffusion constant at face-value and not look too much into it, 'cause its the resultant effect of many forces, and its not scientifically fair to justify the entire frame by just one effective diffusion constant.

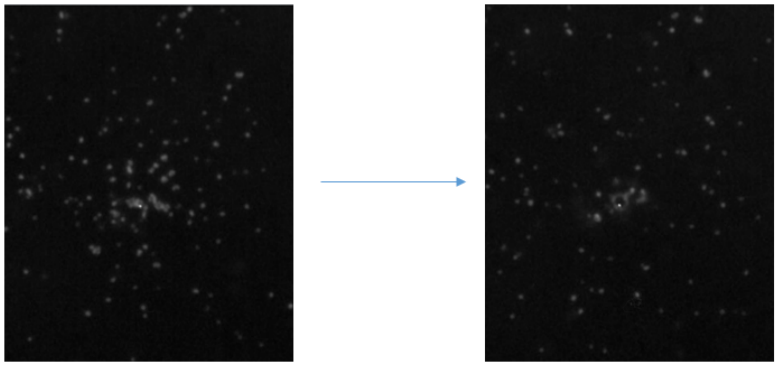

This shows our progress from the when the laser just went on, to when it was just turned off, for the entire sample plane.

The diffusion constant comes out to be 0.018 $\mu m^2/s$. This is larger than the a normal diffusion process for particles of this size and it corresponds to superdiffusive motion. The image is attached here. However it is not as high as the portion where the particles come to trap, a bit away from the laser.

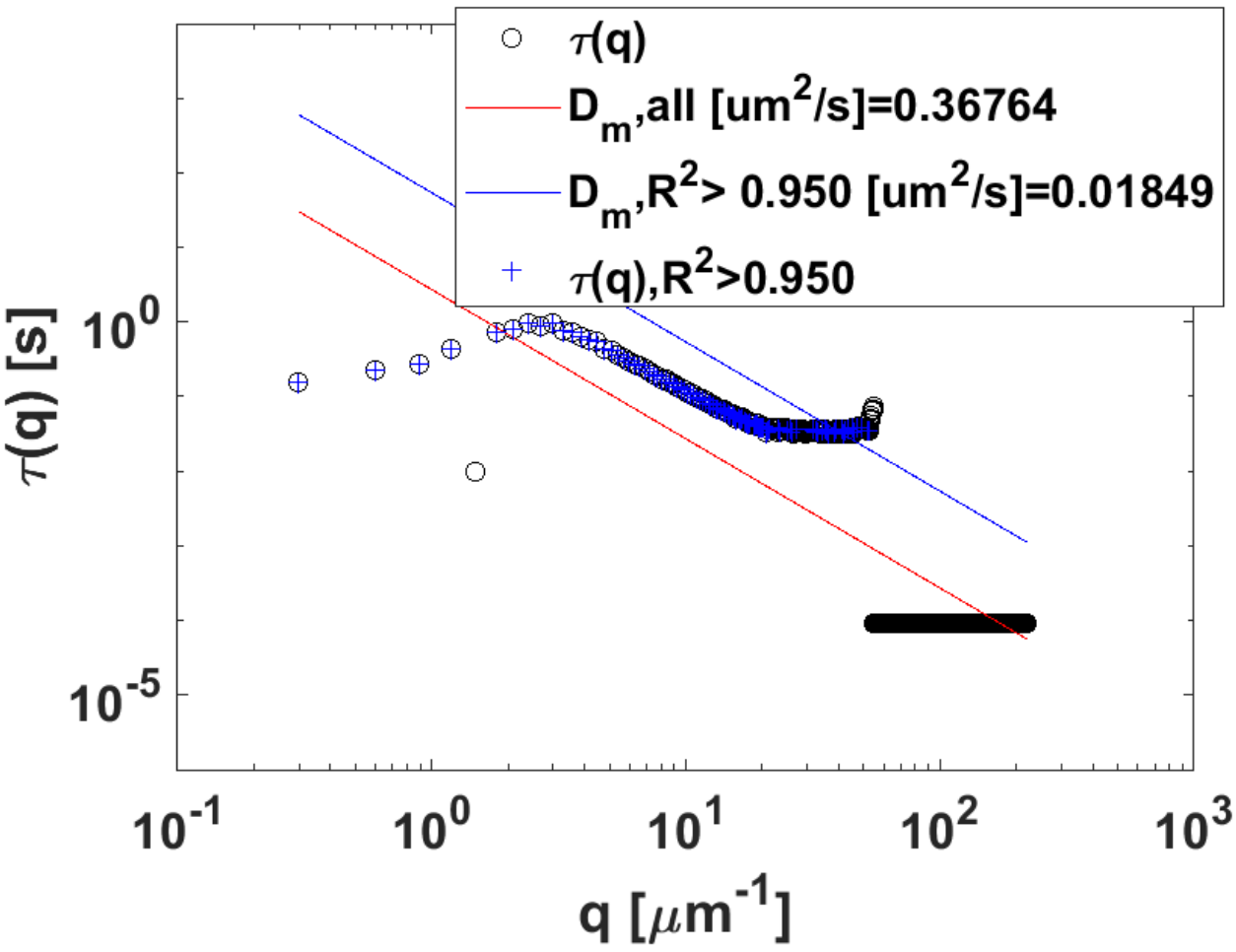

Our range of A(q) and B(q) gives us the actual usable range of q-vectors which are being used throughout the analysis. As long as A>B for a q, it gives us useful information.

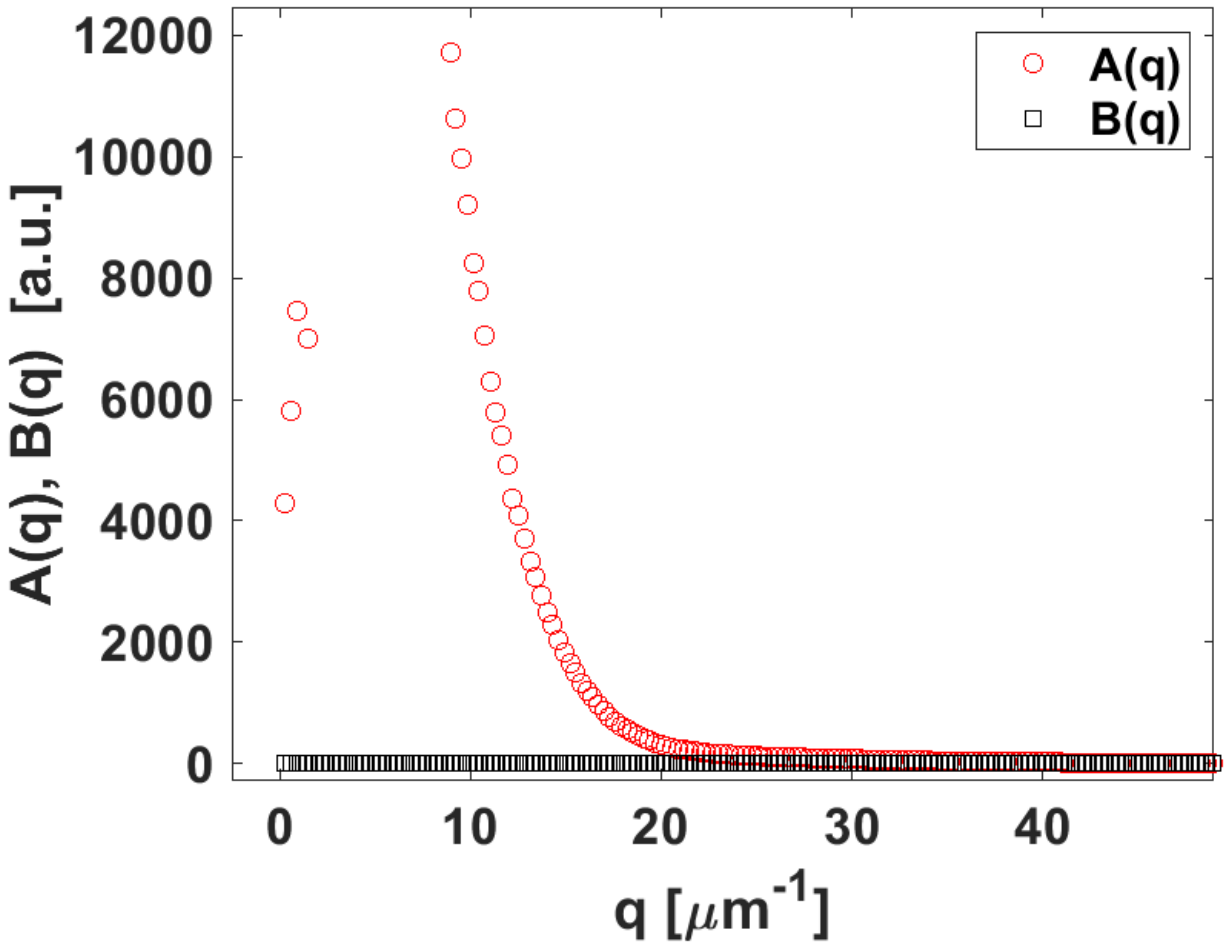

We also give the graph of R^2 vs q, so that we can show that only that range of spatial frequency vectors have been used which are reliable with an NRSME(normalized root mean squared error) of maximum 5 percent, or $R^2 > 95\%$.

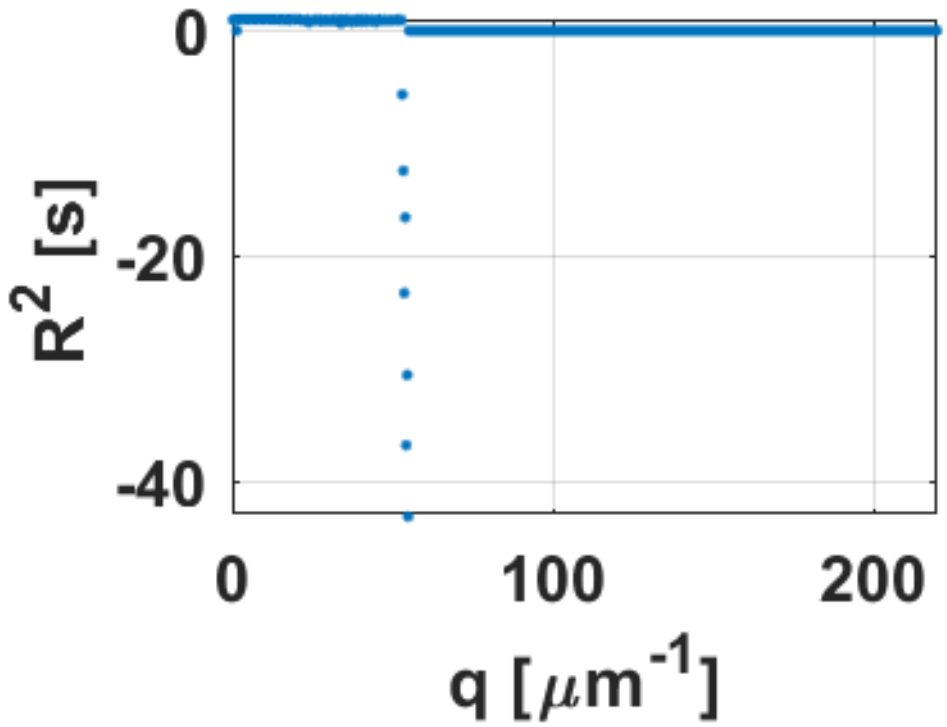

A measure of accuracy of q-vectors used in the analysis.

Although the R^2 value is good for over 200, considering the A and B graph, we analysed till 100 or 10^2 order.

We also include some particular fitting of the D(q,t) vs q at selected time periods, where they fit best and gave us proper diffusion motions.

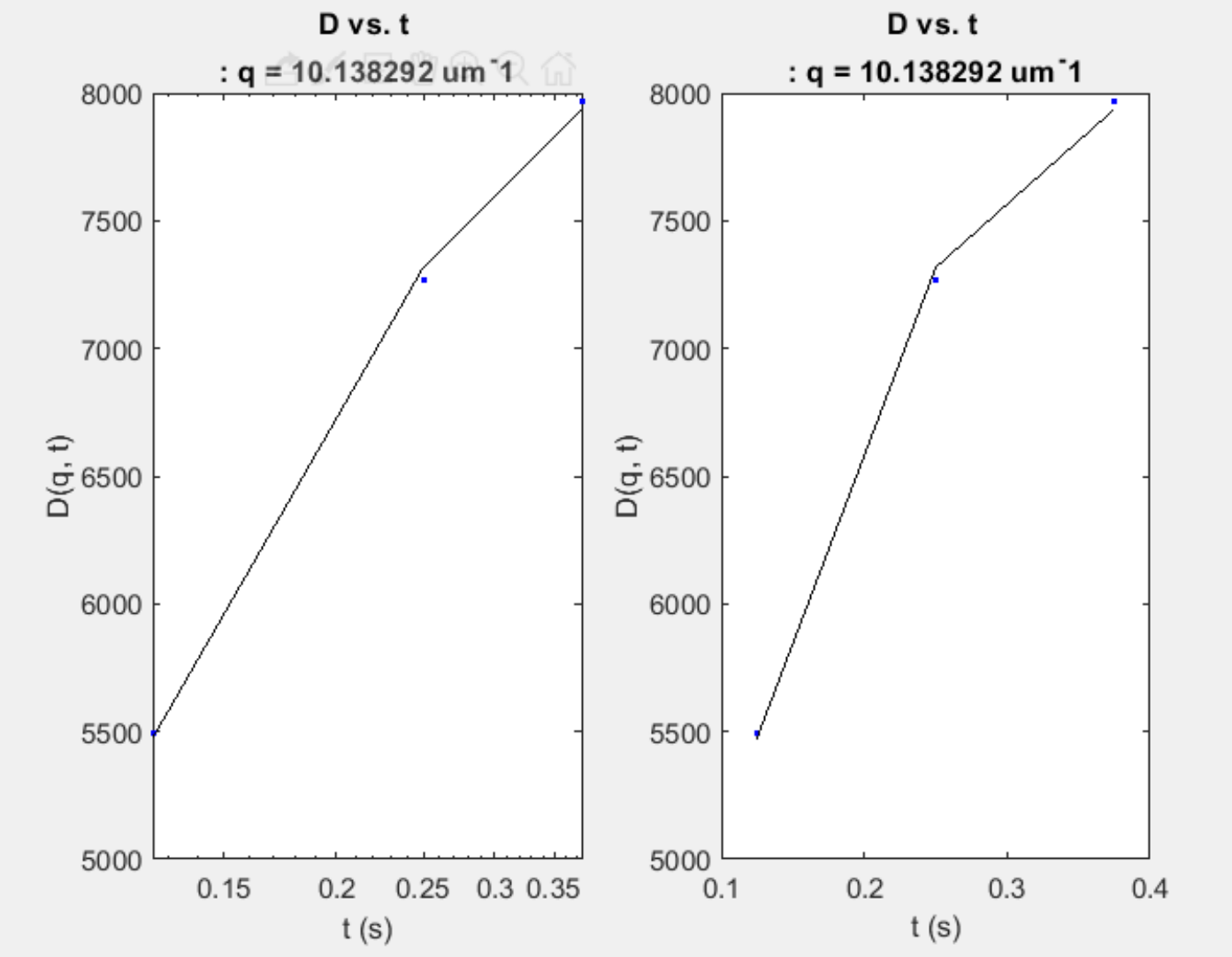

D(q,t) vs q at selected time periods

These are all the data that we processed.

Chapter 4

Conclusion

Thus having studied quite an interesting system, we can see that that various motions can get highlighted depending on the strength of the forces in play. Here since we are considering extremely small particles and quite a dense number of them, DDM naturally became the ideal process to study it. This study still has potential that is unexplored here, which includes trap stiffness and introducing other soft matter into this system. This technique is an upcoming technique and all sorts of possibilities are getting realized eventually. Here we saw that irrespective of the instruments used, we achieved major computational results that could clearly differentiate between the various processes undergoing among the thousands of nanoparticles in the system. Fourier imaging has always been a powerful technique and differential dynamic microscopy uses the best of its abilities. There are some limitations currently which include it not being recorded in real time, which may lead to a repetitive taking of the data due to some error we may realise post processing. It also involves considerable computational power, however we can crop images and deacrease their quality without having to compromise their information because all the images will be likely affected in the same way, and taking their difference will cancel them all out. Some followup to this project might be in preparing various concentrations and calculating trap stiffness, or in the other samples, when traps were'nt formed but the process was still subdiffusive near the trap. So careful measurements might lead to formation of unique traps or filters which alter the flow of soft matter in the system according to our needs.

Bibliography

[1] A. Ashkin, "Acceleration and trapping of particles by radiation pressure," *Physical review letters*, vol. 24, no. 4, p. 156, 1970.

[2] J. R. Meyer-Arendt, *Introduction to classical and modern optics*. Prentice-Hall, 1984.

[3] "Blue sky and rayleigh scattering." `http://hyperphysics.phy-astr.gsu.edu/hbase/atmos/blusky.html#c4`. (Accessed on 06/03/2021).

[4] C. Raman and K. Krishnan, "hν o hν," *Nature*, vol. 121, p. 501, 1928.

[5] "Raman scattering." `http://hyperphysics.phy-astr.gsu.edu/hbase/atmos/raman.html`. (Accessed on 06/04/2021).

[6] E. Albuquerque, "Theory of brillouin scattering by stoneley waves," *Journal of Physics C: Solid State Physics*, vol. 13, no. 13, p. 2623, 1980.

[7] L. Brillouin, "Diffusion de la lumière et des rayons x par un corps transparent homogène," in *Annales de physique*, vol. 9, pp. 88–122, 1922.

[8] "Rp photonics encyclopedia - brillouin scattering, nonlinearity, optical fibers, threshold." `https://www.rp-photonics.com/brillouin_scattering.html#:~:text=Brillouin%20scattering%20is%20an%20effect,backward%20direction%2C%20and%20a%20phonon.` (Accessed on 05/24/2021).

[9] C. Wolff, M. Smith, B. Stiller, and C. Poulton, "Brillouin scattering—theory and experiment: tutorial," *JOSA B*, vol. 38, no. 4, pp. 1243–1269, 2021.

[10] D. Cotter, "Stimulated brillouin scattering in monomode optical fiber," *Journal of Optical Communications*, vol. 4, no. 1, pp. 10–19, 1983.

[11] A. S. Pine, "Brillouin scattering study of acoustic attenuation in fused quartz," *Physical Review*, vol. 185, no. 3, p. 1187, 1969.

[12] E. Garmire, "Applications of lasers, essay in fundamentals of physics, hall iday, resnick and walker," 1993.

[13] K. Moller, "Optics. mill valley," 1988.

[14] G. Benedek, J. Lastovka, K. Fritsch, and T. Greytak, "Brillouin scattering in liquids and solids using low-power lasers," *JOSA*, vol. 54, no. 10, pp. 1284–1285, 1964.

[15] S. Ghosh and A. Ghosh, "Next-generation optical nanotweezers for dynamic manipulation: from surface to bulk," *Langmuir*, vol. 36, no. 21, pp. 5691–5708, 2020.

[16] A. Ashkin, J. M. Dziedzic, J. E. Bjorkholm, and S. Chu, "Observation of a single-beam gradient force optical trap for dielectric particles," *Optics letters*, vol. 11, no. 5, pp. 288–290, 1986.

[17] I. A. Favre-Bulle, A. B. Stilgoe, E. K. Scott, and H. Rubinsztein-Dunlop, "Optical trapping in vivo: theory, practice, and applications," *Nanophotonics*, vol. 8, no. 6, pp. 1023–1040, 2019.

[18] L. Lin, M. Wang, X. Peng, E. N. Lissek, Z. Mao, L. Scarabelli, E. Adkins, S. Coskun, H. E. Unalan, B. A. Korgel, *et al.*, "Opto-thermoelectric nanotweezers," *Nature photonics*, vol. 12, no. 4, pp. 195–201, 2018.

[19] A. V. Bayles, T. M. Squires, and M. E. Helgeson, "Dark-field differential dynamic microscopy," *Soft Matter*, vol. 12, no. 8, pp. 2440–2452, 2016.

[20] R. Cerbino and V. Trappe, "Differential dynamic microscopy: probing wave vector dependent dynamics with a microscope," *Physical review letters*, vol. 100, no. 18, p. 188102, 2008.

[21] F. Giavazzi and R. Cerbino, "Digital fourier microscopy for soft matter dynamics," *Journal of Optics*, vol. 16, no. 8, p. 083001, 2014.

[22] R. Borsali and R. Pecora, "Soft matter: Scattering," *Imaging and Manipulation (Springer, Berlin, 2008)*, 2008.

[23] B. J. Berne and R. Pecora, *Dynamic light scattering: with applications to chemistry, biology, and physics*. Courier Corporation, 2000.

[24] F. Giavazzi, D. Brogioli, V. Trappe, T. Bellini, and R. Cerbino, "Scattering information obtained by optical microscopy: differential dynamic microscopy and beyond," *Physical Review E*, vol. 80, no. 3, p. 031403, 2009.

[25] P. Lee and D. Meisel, "Adsorption and surface-enhanced raman of dyes on silver and gold sols," *The Journal of Physical Chemistry*, vol. 86, no. 17, pp. 3391–3395, 1982.

[26] C. Kan, X. Zhu, and G. Wang, "Single-crystalline gold microplates: synthesis, characterization, and thermal stability," *The Journal of Physical Chemistry B*, vol. 110, no. 10, pp. 4651–4656, 2006.

***